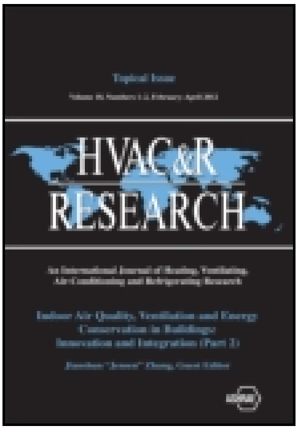

HVAC&R Research
Publication details, including instructions for authors and subscription information:
http://www.tandfonline.com/loi/uhvc20

Optimal coordination of heat pump compressor and fan speeds and subcooling over a wide range of loads and conditions

Tea Zakula [a], Peter Armstrong [b] & Leslie Norford [a c]
[a] Building Technology Program, Massachusetts Institute of Technology (MIT), Cambridge, MA
[b] Mechanical Engineering Program, Masdar Institute of Science and Technology, Abu Dhabi, United Arab Emirates
[c] Department of Architecture, Massachusetts Institute of Technology (MIT), Cambridge, MA
Accepted author version posted online: 10 Aug 2012.Version of record first published: 14 Nov 2012.

To cite this article: Tea Zakula, Peter Armstrong & Leslie Norford (2012): Optimal coordination of heat pump compressor and fan speeds and subcooling over a wide range of loads and conditions, HVAC&R Research, 18:6, 1153-1167

To link to this article: http://dx.doi.org/10.1080/10789669.2012.713832

Optimal coordination of heat pump compressor and fan speeds and subcooling over a wide range of loads and conditions

Tea Zakula,[1,*] Peter Armstrong,[2] and Leslie Norford[1,3]
[1]*Building Technology Program, Massachusetts Institute of Technology (MIT), Cambridge, MA*
[2]*Mechanical Engineering Program, Masdar Institute of Science and Technology, Abu Dhabi, United Arab Emirates*
[3]*Department of Architecture, Massachusetts Institute of Technology (MIT), Cambridge, MA*
Corresponding author e-mail: tzakula@mit.edu

Advanced cooling systems with high-temperature cooling (sensible only), night precooling, and highly efficient variable-speed compressors, fans, and pumps can benefit from on-line model predictive control to find and continually update optimal daily (or weekly) precooling sequences. As a part of the model predictive control, it is desirable to use optimized plant-specific control laws to match compressor, fan, and pump speeds to required capacity. A previous work presented a modular heat pump model that simulated steady-state performance over wide ranges of lift (external pressure ratios from <1 to 6) and capacity (10:1 turndown) that could be explored in the search for optimal solutions. This article describes the adaptive grid search technique used to map optimal heat pump performance as a function of the capacity and indoor and outdoor temperatures. The grid search finds optimal condenser and evaporator airflows and optimal subcooling at each operating point. The method is illustrated for a number of cases, including two-compressor systems and refrigerants R410A, R600 (propane), and R717 (ammonia). The non-linearity of optimal fan-speed control laws is demonstrated. The impact of zero subcooling with respect to optimal subcooling is assessed for the single compressor machines. The specific power at optimal fan speeds, as a function of capacity and indoor–outdoor temperature, is compared for R410A, propane, and ammonia-charged machines. Finally, the question of optimal sizing of optimally controlled variable-speed heat pumps is explored, and it is shown that modest oversizing is desirable. These findings suggest that the relative sizing of heat pump components—compressor, compressor motor, condenser, and evaporator—as well as the sizing of the heat pump itself relative to design load, may benefit from a thorough reassessment of current practice.

Introduction

One attractive way to achieve efficient cooling in buildings is to combine efficient, optimally controlled thermal energy storage (TES); high-temperature distribution, such as chilled beams; and a cooling plant that operates efficiently over a wide range of lift and part-load fractions. This combination of components and controls may be called a low-lift cooling system (LLCS). In simulations with idealized TES, annual cooling system energy savings of up to 75% were found compared to a baseline

Received February 22, 2012; accepted June 25, 2012
Tea Zakula, Student Member ASHRAE, is PhD Candidate. **Peter Armstrong, PhD**, Member ASHRAE, is Associate Professor. **Leslie Norford, PhD**, Member ASHRAE, is Professor.

HVAC&R Research, 18(6):1153–1167, 2012.
ISSN: 1078-9669 print / 1938-5587 online
DOI: 10.1080/10789669.2012.713832

ASHRAE 90.1-2004 VAV system (Jiang et al. 2007; Armstrong et al. 2009a, 2009b; Katipamula et al. 2010). Initial verification of these results was provided by Gayeski (2010) for a typical summer week for Atlanta and Phoenix in a climate chamber experiment using the identical outdoor unit (compressor, condenser, and fan) for both the low-lift and baseline configurations. Since optimization and control are critical for maximizing the benefits of the LLCS, an important part of the low-lift cooling technology is model predictive control, an algorithm that optimizes the system's operation given a thermal response model of the building and weather forecasts. Another key optimization question is the coordination of condenser and evaporator fan and/or pump speeds with compressor speed to satisfy any given load under any given conditions. This process is known in the HVAC literature as *static optimization* (ASHRAE 2011, Chap. 42). Although the use of empirical data (Gayeski 2010) is unavoidable for modeling building transient thermal response, heat pump performance can, in principle, be more easily and reliably characterized by the use of engineering models (Gayeski et al. 2011; Verhelst et al. 2012). However, heat pump manufacturers' data are often only available for a limited range of operating conditions and capacity. This makes it nearly impossible to analyze systems that operate outside those conditions or systems that are still commercially unavailable. Therefore, to perform static optimization, a heat pump model that is accurate, yet computationally inexpensive, is required.

The most detailed physics-based heat pump model found in the static optimization literature is that developed by Armstrong et al. (2009a) (Jiang et al. 2007). Two optimization variables are the evaporating and condensing temperatures, which can then be related to the optimal evaporator fan, condenser fan, and compressor speeds. The model assumes constant evaporating and condensing temperatures without evaporator superheating, condenser subcooling, or heat pump pressure drops. It also assumes constant conductance (U-value) for the evaporator and condenser, independent of refrigerant and air/water flow rates. Zakula et al. (2011) showed that even neglecting pressure drops can lead to serious errors in power consumption predictions, and therefore, this model would need to be extended for more accurate performance predictions. There are numerous physical models found in the literature that do not perform optimization but that do calculate steady-state heat pump performance and, hence, could potentially be adopted for optimization purposes. However, they vary from complex models that are computationally expensive and require a large number of input parameters to models that are similar to Armstrong et al.'s (2009a) model, in that they are relatively simple and fast but do not take into account certain important phenomena. A more detailed literature review on heat pump modeling is given in Zakula (2010).

Though they do not describe the optimization of a heat pump's performance, related works on the optimization of large chiller plants can be found in the literature. Lau et al. (1985) developed a TRNSYS (transient system simulation program; Klein et al. 2010) model to analyze different control strategies for an existing chiller plant with four centrifugal chillers, a cooling tower, and chilled water tanks. For a given cooling load and wet-bulb temperature, the cooling tower fan speed, condenser pump flow, and number of chillers were optimized for minimal power consumption. The power consumption of each chiller is characterized as a function of the cooling load, leaving chilled water temperature, and leaving condenser water temperature using curve fits to manufacturer's data. Braun et al. (1987a) investigated the performance and optimal control of a large chiller plant equipped with a cooling tower. A simplified model was used to find near-optimal control, with the cooling tower airflow and condenser water flow rates as the control variables. For an individual chiller, measured data from the existing plant were fit to curves that define the chiller power as a function of the cooling load and temperature difference between the leaving condenser and chilled water flows. In subsequent work (Braun et al. 1989), the system was extended to include the chilled water loop and the air handlers with the five independent control variables of supply air set temperature, chilled water set temperature, cooling tower airflow, condenser water flow, and the number of operating chillers. Braun's more recent work on chiller plant optimization (Braun 2007) analyzed near-optimal control strategies for a hybrid cooling plant powered by electricity and natural gas. The optimization objective function was the operating cost, which includes the electrical and gas energy cost, electrical demand cost, and maintenance cost. For a given cooling load, return air (zone) temperature, wet-bulb temperature, and state of charge, the model of King and Potter (1998) optimized chilled water and supply air temperature set-points for the lowest system power consumption, including the chiller, pumps,

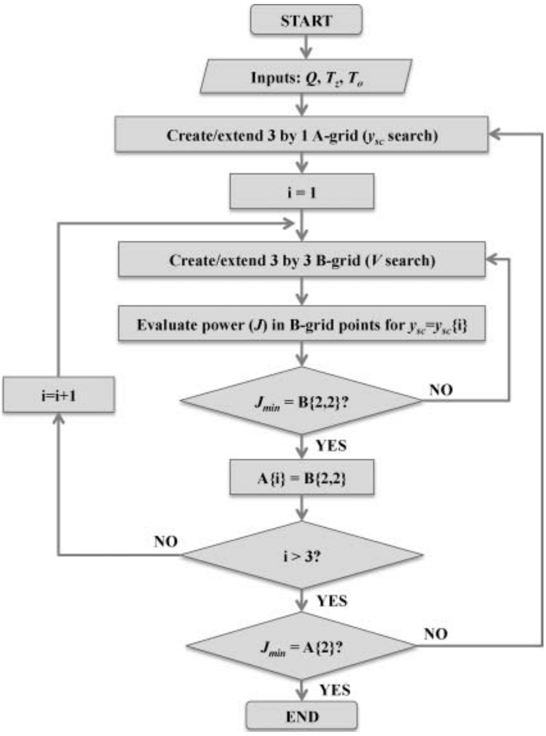

Figure 1. Grid search optimization algorithm.

cooling-tower fan, and supply- and return-air fans. Similar to the previous chiller plant optimization models, performance of an individual chiller is captured using curve fits to manufacturer's data. Jiang and Reddy (2007) developed a general methodology for optimization of HVAC&R plants and showed its application on a cooling plant that consists of three chillers (one of which is absorption chiller) and three variable-speed cooling towers. The semi-empirical Gordon–Ng model and effectiveness-NTU (Number of Transfer Units) model were used to model chillers and cooling towers. Given total cooling load and required supply temperature and flow rate, the load allocated to each chiller and cooling tower outlet water temperature of each chiller were used as optimization variables.

The objective of this study is to use optimization to better understand the extent to which heat pump design and control improvements can impact the annual energy use of advanced cooling systems.

Model description

Optimization is performed using the steady-state heat pump model developed by Zakula et al. (2011) that can simulate the performance of different heat pump types, such as air-to-air heat pumps and air- and water-cooled chillers. Two evaporator sub-models that describe finned-tube air-to-refrigerant and brazed-plate water-to-refrigerant heat exchangers are modeled using the heat balance equations and ε-NTU method for evaporating and superheating regions. The condenser is modeled in a similar manner, except it consists of desuperheating, condensing, and subcooling regions. The heat transfer coefficients are calculated separately for the air/water stream and two-phase and single-phase refrigerant flows. The compressor sub-model calculates the compressor speed, compressor power, and discharge temperature for a given mass flow rate, compressor inlet state, and outlet pressure. The shaft

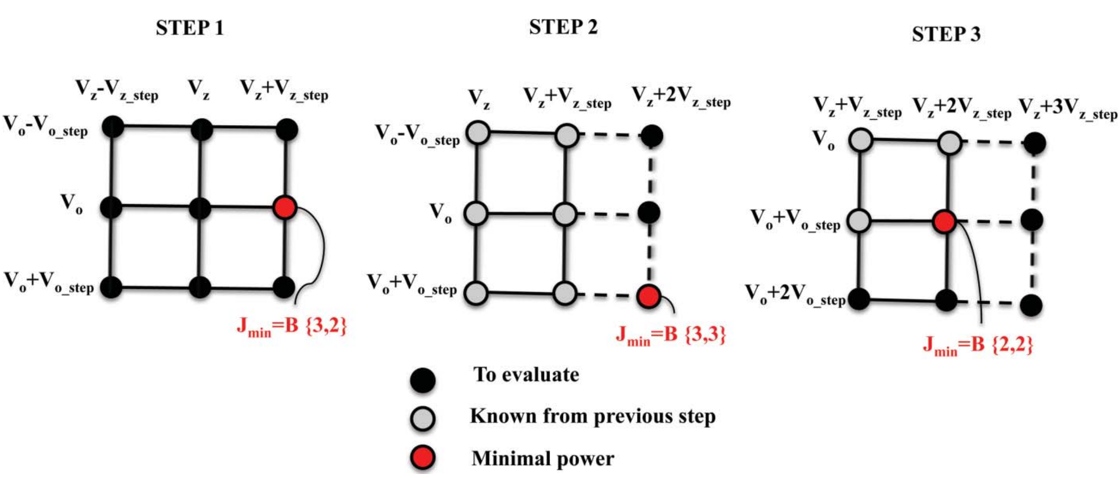

Figure 2. Search loop for the optimal airflow (B-grid) (color figure available online).

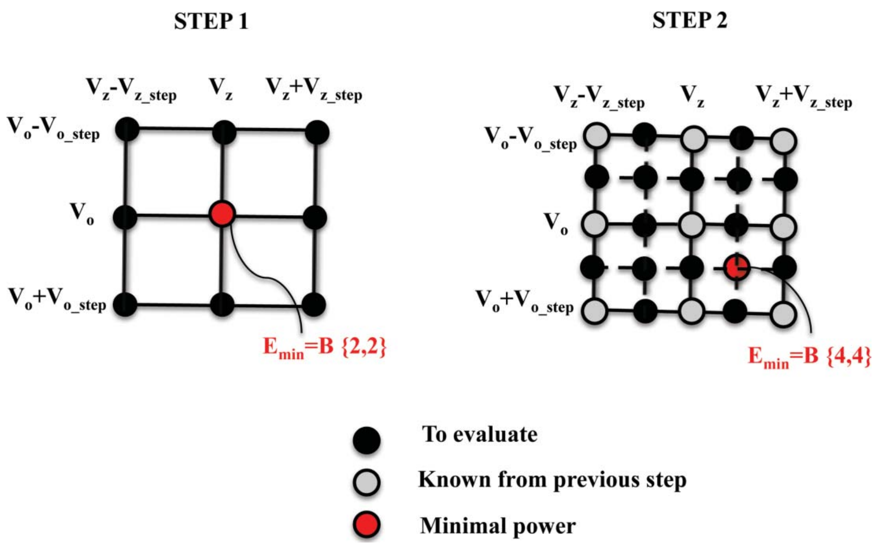

Figure 3. Grid search step adaptation (color figure available online).

speed is calculated using a volumetric efficiency model, and the compressor power is calculated as the power required for isentropic work, corrected by the combined efficiency that takes into account losses in the compressor and motor. The compressor outlet temperature is calculated from the compressor heat balance, through which the lubricating oil is assumed to pass in a constant mass fraction. A liquid receiver is assumed to maintain the necessary charge balance, which is not modeled. The heat pump model takes into account pressure drops in refrigerant piping and heat exchangers, the dependence of heat transfer coefficients on flow rates, superheating in the evaporator and desuperheating, and subcooling in the condenser. A modular approach offers the possibility of choosing between different simulation options (level of complexity) and makes the model easy to expand and customize. The model can be used for a single-, two-, or variable-speed compressor, a single compressor, multiple parallel compressors, evaporators or condensers, as well as for different refrigerants. The inverse heat pump model with compressor frequency as an input has also been developed and is used to optimize a heat pump with a two-speed compressor. The two-speed heat pump serves as a base case for annual energy consumption assessments presented later.

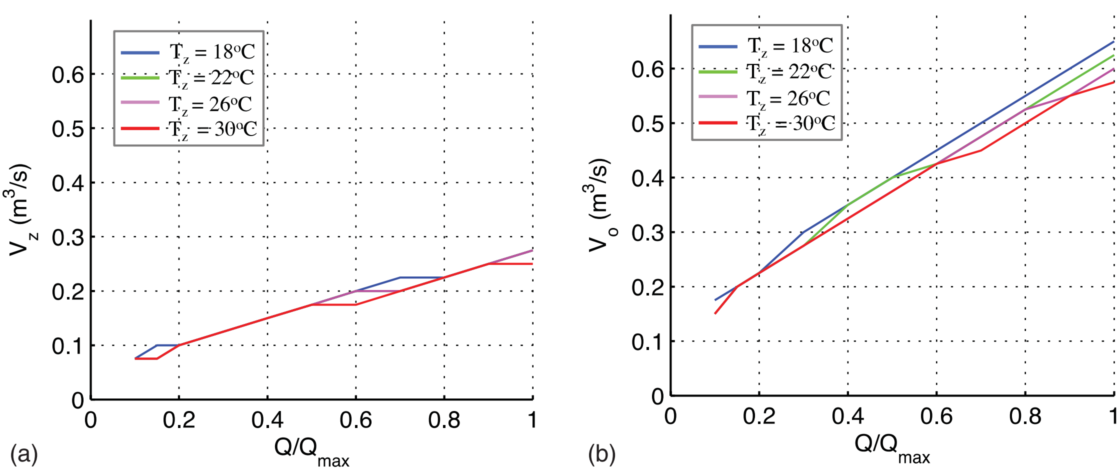

Figure 4. Optimal (a) evaporator and (b) condenser airflow as a function of part-load ratio for T_o = 30°C (86°F) (color figure available online).

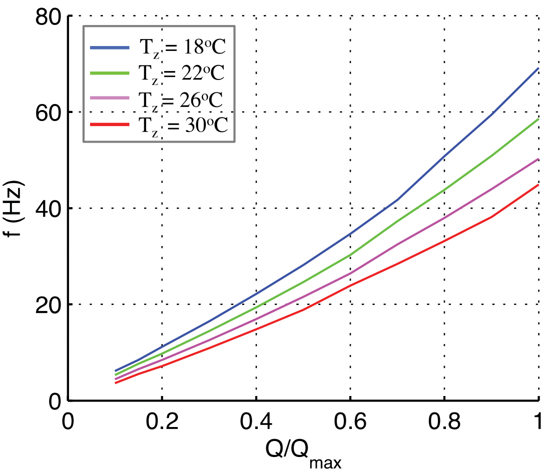

Figure 5. Optimal compressor frequency as a function of part-load ratio for $T_o = 30°C$ (86°F) (color figure available online).

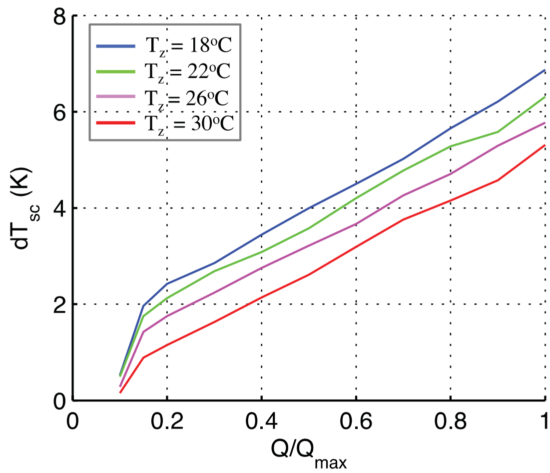

Figure 6. Optimal subcooling as a function of part-load ratio for $T_o = 30°C$ (86°F) (color figure available online).

The optimization input parameters are the cooling load (Q), zone temperature (T_z), and outside temperature (T_o), and the optimization variables are the evaporator airflow rate (V_z), condenser airflow rate (V_o), and condenser area fraction devoted to subcooling (y_{sc}). If one wants to optimize only one or two variables, the other variables need to be given as an input; e.g., one may want to know the performance impact of the optimal subcooling as opposed to zero subcooling, in which case a zero subcooling area is specified and the condenser and evaporator air or water flow rates are optimization variables. All other heat pump operating variables are functions of the optimization variables; in particular, for optimal control, one is mainly interested in the optimal evaporator fan speed, condenser fan speed, and compressor speed. One may also be interested in the related refrigerant mass flow rate, evaporating temperatures and pressures, condensing temperatures and pressures, suction and discharge state, subcooling temperature difference, and total power consumption.

The optimization algorithm, using the grid search method shown in Figure 1, has the advantage of avoiding gradient calculations. Gradient calculations can be computationally expensive and challenging for this type of problem due to non-linearities and possible convergence issues. Furthermore, if a grid step is appropriately chosen, the grid search is more reliable in finding the global minima than the gradient search method.

For each set of conditions (Q, T_z, T_o), there are two loops, the outer loop for the optimal subcooling area ratio search and the inner loop for the optimal flow rates search. The initial 3-by-1 grid (A-grid) and 3-by-3 grid (B-grid) are created for the outer and inner loops, respectively. First, the total power consumption is calculated for each of the nine B-grid points and $y_{sc} = y_{sc}\{1\}$. If the lowest power is anywhere on the B-grid boundaries, the grid is extended according to Figure 2, and total powers are evaluated for new points. The process continues until the lowest power is in the middle B-grid point ($B\{2,2\}$), in which case the algorithm moves to the second A-grid point ($y_{sc}\{2\}$). Similar to the B-grid, if the sub-optimization finishes for all three A-grid points, and the lowest power is on the A-grid

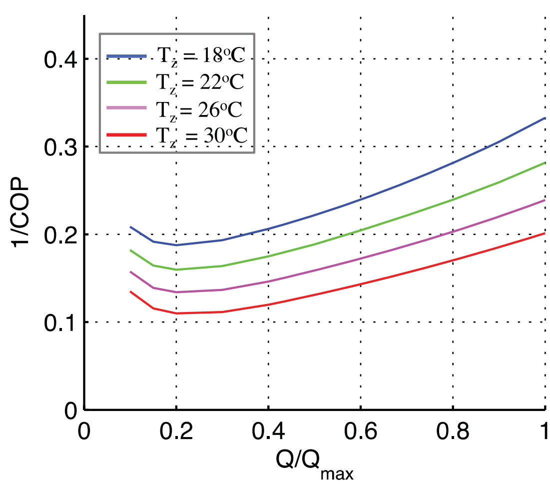

Figure 7. Specific power as a function of part-load ratio for $T_o = 30°C$ (86°F) (color figure available online).

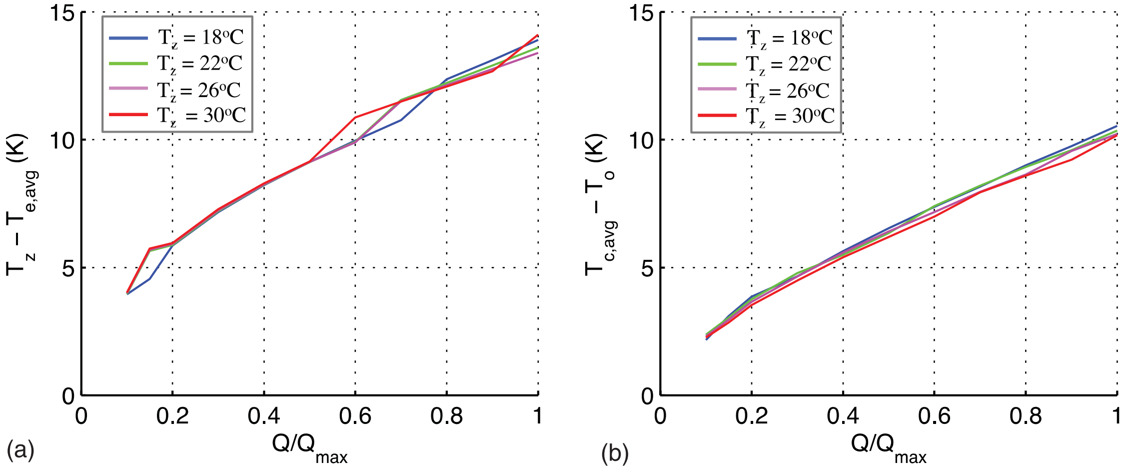

Figure 8. Optimal: (a) zone and evaporating temperature difference and (b) condensing and ambient temperature difference as a function of part-load ratio for $T = 30°C$ (86°F) (color figure available online).

boundaries, the A-grid extends until the optimum is at the middle A-grid point ($A\{2\}$).

The optimization process is further accelerated with the step adaptation, in which after finding the optimal variables with a larger step, a new 5-by-5 B-grid is created using a smaller step (half the large step) and V_{z_opt} and V_{o_opt} as the central grid points (Figure 3). Since the power consumption in 9 points is already known from the previous (large step) grid search, only 16 additional function evaluations are performed. The point with the lowest power is assigned as the final optimal point (new V_{z_opt} and V_{o_opt}). The same is applied for the optimal subcooling search.

Performance map results

For a given cooling rate, outside, and zone temperature, the result of the static optimization provides the optimal set of the evaporator and condenser airflow rates, compressor speed, and subcooling for which the power consumption will be the lowest. To show the broad utility and potential

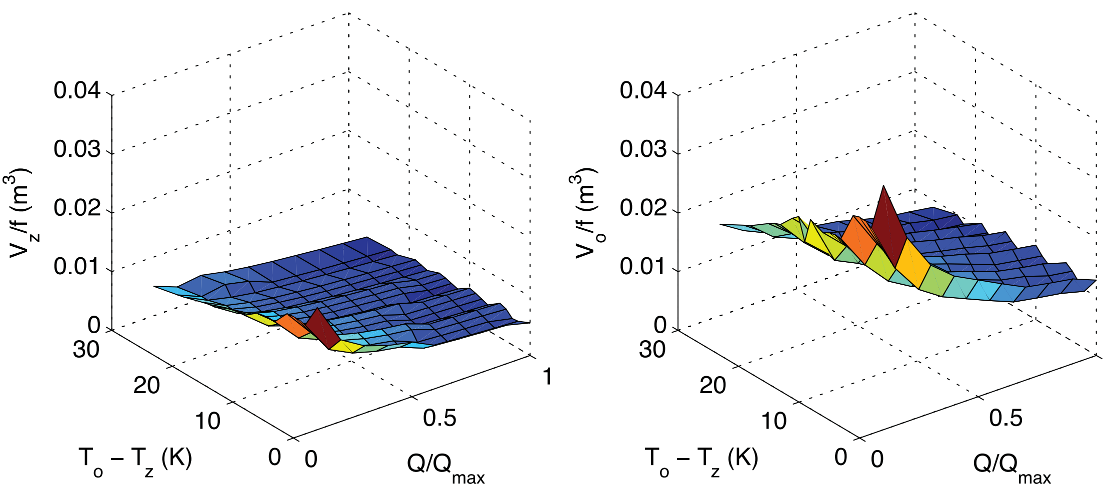

Figure 9. Optimal evaporator and condenser airflow-to-compressor-frequency ratio over a wide range of conditions and loads (color figure available online).

benefits of optimization using a component-based model the optimization is performed for several different scenarios:

a) air-to-air heat pump with a single compressor (variable-speed rolling-piston compressor) and R410A as a refrigerant;
b) air-to-air heat pump with two parallel compressors, evaporators, and condensers (two variable-speed rolling-piston compressors) and R410A as a refrigerant;
c) air-to-air heat pump with a single compressor (variable-speed rolling-piston compressor) and ammonia (R717) as a refrigerant; and
d) air-to-air heat pump with a single compressor (variable-speed rolling-piston compressor) and propane (R600) as a refrigerant.

The optimization is performed with a 0.025 m^3/s (53 cfm) step for the airflows (0–0.3 and 0–0.7 m^3/s [0–635.7 and 0–1483.2 cfm] airflow range for the evaporator and condenser fan, respectively) and a 0.001 step for the condenser area ratio devoted to subcooling.

For the heat pump with a variable-speed compressor and R410A as a working fluid, the optimal set of evaporator and condenser airflow rates (Figure 4), compressor speed (Figure 5), and subcooling (Figure 6), for which the power consumption for cooling (Figure 7) will be the lowest, is shown for the outside temperature $T_o = 30°C$ (86°F). Figure 4 shows that the evaporator and condenser airflows are a strong function of part-load ratios. Furthermore, it was noticed that when optimizing the airflows, the parameter indirectly being optimized is the temperature difference (Figure 8). For a given cooling rate, the optimizer tries to maintain the optimal temperature difference on the evaporator (between the evaporating and air temperature) and the condenser (between the condensing and air temperature), regardless of the zone or ambient temperature. From Figure 7, which shows the specific power as a function of part-load ratios, it can be seen that the heat pump efficiency increases with lower part-load ratios. This raises the question of the appropriate heat pump "external sizing," since with modest oversizing, the heat pump will run at higher efficiencies. However, because there is a cost penalty associated with a size increase, both size and initial cost need to be carefully balanced. The optimal "external sizing" for the lowest energy consumption is discussed later in this article. In addition to "external sizing," which refers to selecting a heat pump capacity appropriate for the load, another interesting topic to be addressed is "internal sizing," which is the sizing of each heat pump component, primarily the evaporator, condenser, and compressor. Although not included as a part of this analysis, the presented heat pump optimization algorithm could be extended to the component-sizing problem given a joint distribution of cooling load and operating conditions.

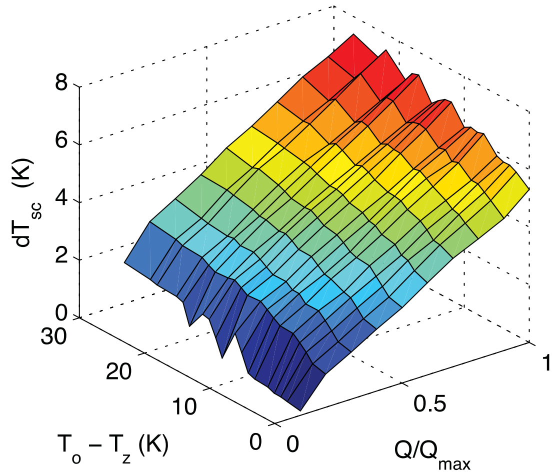

Figure 10. Optimal subcooling over a wide range of conditions and loads (color figure available online).

The optimal results are presented here over a wide range of loads (0.1–1 part-load ratio) and temperature differences (0°C–30°C [0°F–54°F] difference between the zone and ambient). Although Figure 4 indicates nearly linear trends for

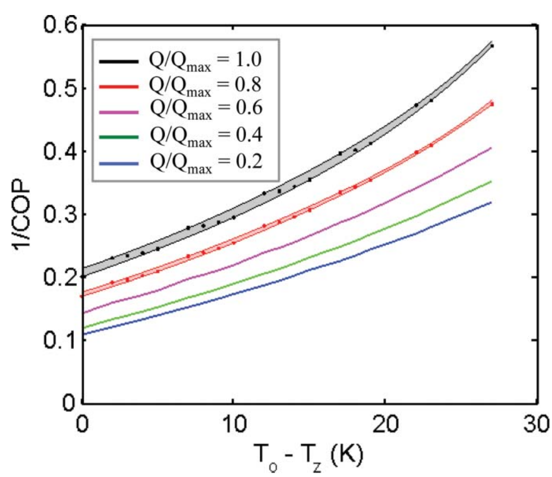

Figure 11. Specific power over a wide range of conditions and loads (color figure available online).

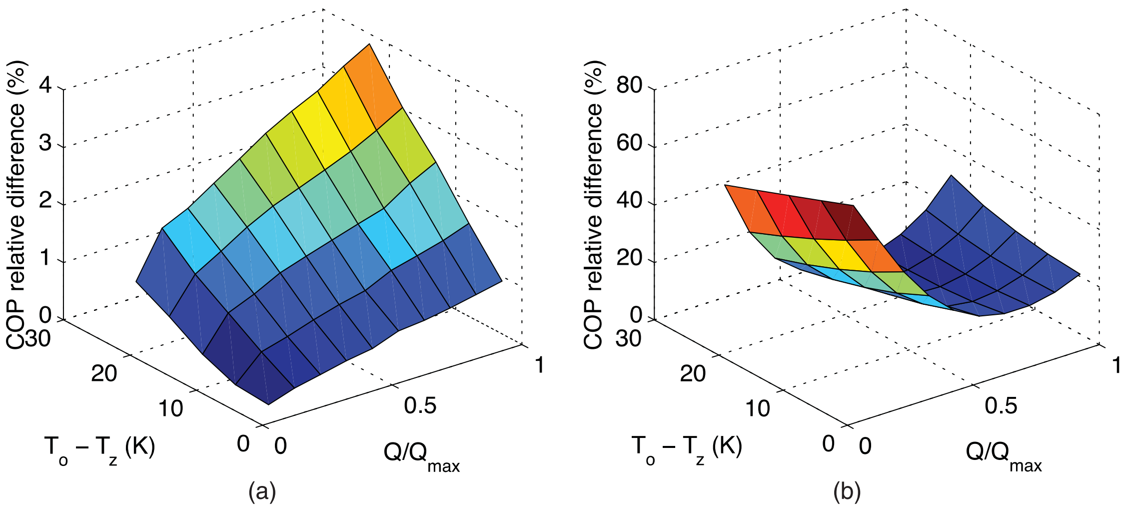

Figure 12. COP relative difference: (a) optimal versus zero subcooling case and (b) optimal versus fixed air flow and zero subcooling case, all for $T_z = 22°C$ (71.6°F) (color figure available online).

the evaporator and condenser airflows, it can be seen from Figure 9 that the same is not true for the optimal airflow-to-compressor-frequency ratio. Similar to optimal airflows, Figure 10 shows a strong dependence of the optimal subcooling on the part-load ratio. Finally, it can be seen from Figure 11 that the optimal specific power is almost solely a function of part-load ratio and (for a moderate range of evaporating temperature) of temperature differences between the zone and outside. This is in agreement with the study done by Braun et al. (1987b) that concluded that the chiller power consumption is primarily a function of cooling load and the temperature difference between the leaving condenser and chilled water streams. It is important to point out that the optimal evaporator airflows at high part-load ratios are significantly higher than the maximum feasible for the specific heat pump (the airflow rate at the maximum evaporator fan speed was around 0.15 m^3/s [317.8 cfm] for the real heat pump). Because manufacturers primarily optimize this type of heat pump for simultaneous sensible cooling and dehumidification, in which the heat pump would run with much lower evaporator fan speeds, their use for only sensible cooling results in fan speeds that are far from optimal. The consequence of this for the total energy consumption is described later in an example.

Subcooling has been used as one of the optimization variables considering that some heat pump manufacturers already do control subcooling by placing an additional valve between the condenser and liquid receiver. The impact of optimal subcooling with respect to zero subcooling is assessed. Figure 12a shows that the coefficient of performance (COP) differences, although relatively small, increase for higher part-load ratios and temperature differences. As a result, the average annual COP of a system that operates at lower part-load ratios would be much less influenced by non-optimized subcooling compared to prevailing systems that deliver most of their annual cooling effect at high

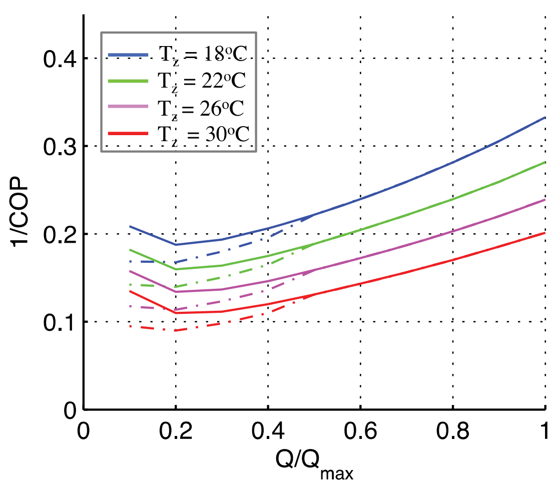

Figure 13. Specific power as a function of part-load ratio for single-compressor machine (solid line) and two-compressor machine with each compressor sized for half Q_{max} (dashed line), all for $T_o = 30°C$ (86°F). Specific power is the same for both machines above ~50% part-load (color figure available online).

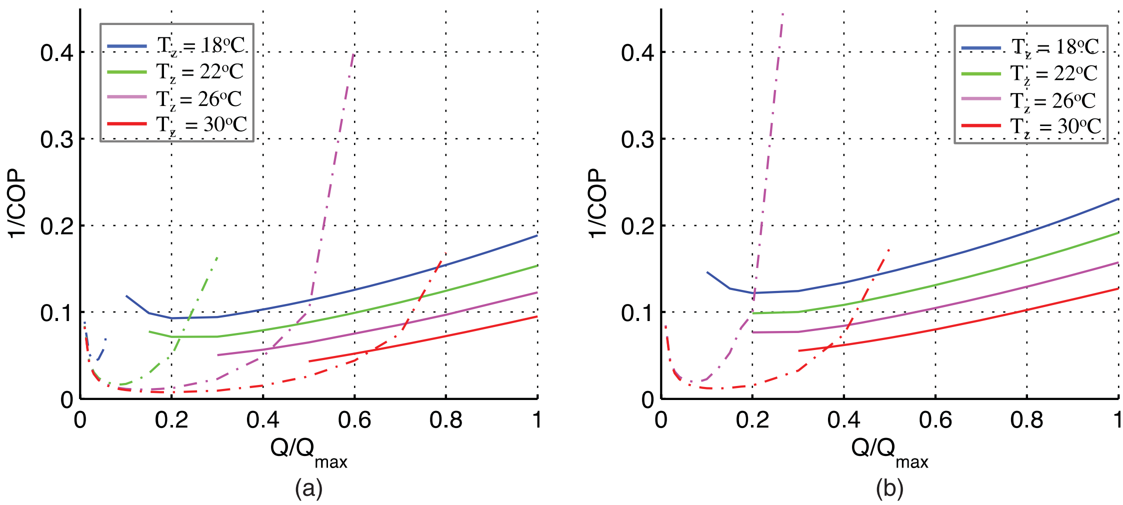

Figure 14. Economizer mode (dashed line) and compressor mode (solid line) for: (a) $T_o = 15°C$ (59°F) and (b) $T_o = 20°C$ (68°F) (color figure available online).

part-load ratios. The COP relative differences in Figure 12a are calculated as

$$\text{COP relative difference} = \frac{\text{COP}_{\text{optimized}} - \text{COP}_{\text{zero subcooling}}}{\text{COP}_{\text{optimized}}}. \qquad (1)$$

An additional analysis was done to assess the impact of the optimized airflows with respect to fixed airflows. Fixed airflows were set to the maximum feasible for the specific heat pump (0.15 and 0.77 m^3/s [317.8 and 1631.5 cfm] for the evaporator and condenser fan, respectively), and the subcooling was set to zero. The results (Figure 12b) show significant differences in the specific power between the optimal and non-optimal cases. This leads to the conclusion that optimizing the airflows plays a significant role in the heat pump performance and that heat pumps optimized for simultaneous sensible cooling and dehumidification can significantly underperform when used for sensible cooling only. The COP relative differences in Figure 12b are calculated as

$$\text{COP relative difference} = \frac{\text{COP}_{\text{optimized}} - \text{COP}_{\text{non-optimized}}}{\text{COP}_{\text{optimized}}}. \qquad (2)$$

It can be seen in Figure 7 that due to inverter losses, the specific power increases for part-load ratios less than 0.2. The inverter losses account for a small portion of the total power at higher part-load ratios but become more important as the cooling load decreases. Recently, manufacturers have started to design heat pumps with two, rather than one, variable-speed compressors, which can help to avoid high inverter losses at lower part-load ratios and result in better overall heat pump performance. This case has been analyzed by optimizing the heat pump with 2× scaling of evaporators, condensers, and piping and two variable-speed rolling-piston compressors. The optimization algorithm tests both cases and decides if it is more efficient to run both or just one of the compressors. The results of the analysis (Figure 13) show that the heat pump design with two parallel compressors can significantly improve the performance at low part-load ratios by running only one of the two inverter-compressor subsystems.

When the outside temperature is lower than the zone temperature, a heat pump can run in an economizer mode, in which only the evaporator and condenser fans are running and the compressor is turned off. In some cases, liquid may flow from the condenser to evaporator by gravity, while in others, the flow may be assisted by a small efficient hermetic pump (New Technology Demonstration Program [NTDP] 1994). Having a lower outside temperature, however, does not necessarily imply that running in the economizer mode is more energy efficient. For small temperature differences relative to a part-load ratio, the total sum of the fan and compressor power

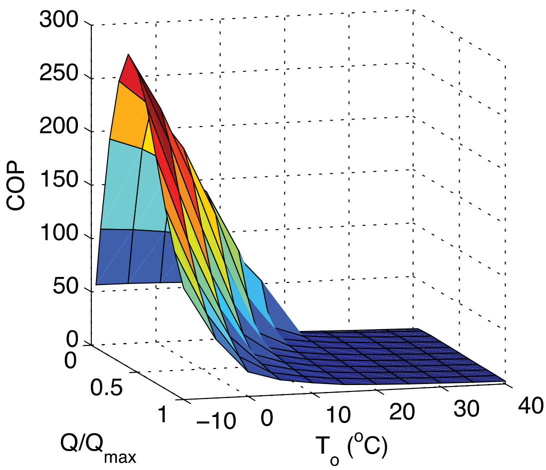

Figure 15. Combined COP (compressor and economizer mode) for $T_z = 22°C$ (71.6°F) (color figure available online).

can be lower than the sum of fan powers when operating in the economizer mode due to high fan speeds. Therefore, without having detailed heat pump maps for both modes (Figure 14), it is hard to develop an appropriate control algorithm that regulates switching between the two. Figure 14a illustrates the slope discontinuity, where the optimal compressor-mode and economizer-mode performance surfaces intersect, and Figure 14b shows how the intersection moves for different outside temperatures. The combined heat pump map is created (Figure 15) using the optimization results and selection of the least power mode when $T_o < T_z$.

The heat pump model and the optimization algorithm can also be used to analyze how changing refrigerants might influence the heat pump performance. When switching to refrigerants other than R410A, the heat pump geometry (primarily the compressor displacement volume and refrigerant piping) was adapted to account for differences in density and heat of vaporization. The compressor displacement volume is scaled using

$$D_{\text{refrigerant}} = D_{R410A} \frac{\rho_{R410A}}{\rho_{\text{refrigerant}}} \frac{h_{lg,410A}}{h_{lg,\text{refrigerant}}}. \qquad (3)$$

The largest pressure drop in the evaporator that corresponds to the 4°C (7.2°F) drop in the saturation temperature (at $T_z = 18°C$ [64.4°F], $T_o = 45°C$ [113°F], and $Q = Q_{\max}$) for R410A was used to find the appropriate scaling factors for the refrigerant piping. The scaling factors found to give the pressure drops that correspond to the same 4°C (7.2°F) drop in the saturation temperature are 0.90 for ammonia and 1.37 for propane. The relative differences in the COP for different refrigerants are shown in Figure 16. The COP relative differences in Figure 16 are calculated as

$$\text{COP relative difference} = \frac{\text{COP}_{\text{refrigerant}} - \text{COP}_{R410A}}{\text{COP}_{R410A}}. \qquad (4)$$

The results show higher COP values for propane and ammonia compared to R410A, which is in agreement with the results of theoretical performance analysis for different refrigerants (ASHRAE

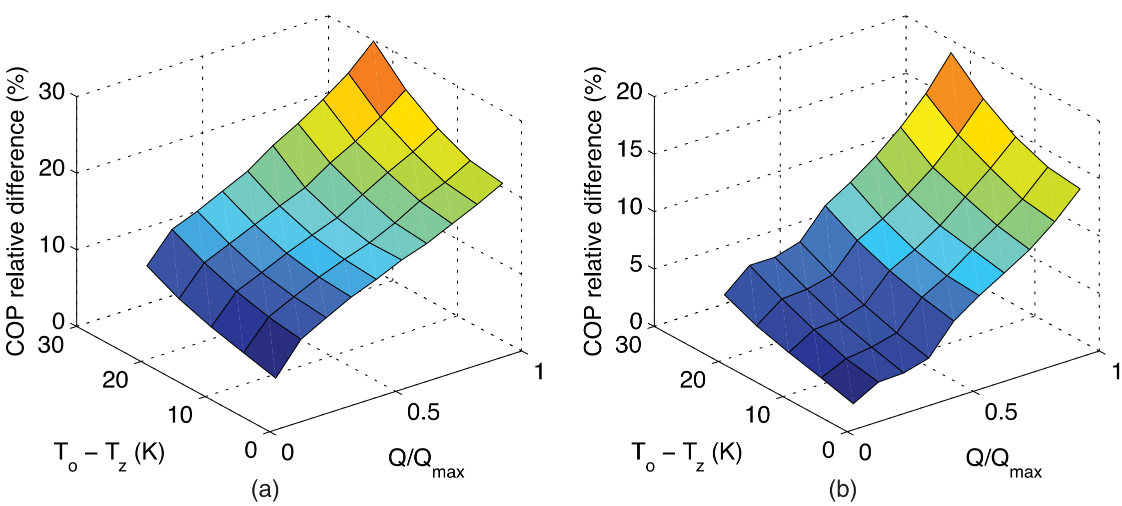

Figure 16. COP relative difference for: (a) ammonia versus R410A case and (b) propane versus R410A case, all for $T_z = 22°C$ (71.6°F) (color figure available online).

2009; Chap. 29, Table 9). Differences in the COP of a theoretical Rankine cycle are caused by throttling-induced irreversibility and additional work required for the superheated-vapor horn (Domanski 1995). For refrigerants operating closer to the critical point, as in the case of R410A, these irreversibilities are higher. Differences due to suction density and enthalpy of vaporization have been largely eliminated by scaling the heat exchanger (HX) channels, compressor displacement, and interconnect piping.

Annual performance results

This section demonstrates how switching to a heat pump with a single two-speed compressor, two parallel compressors, different refrigerants, or a heat pump with non-optimal airflows or non-optimal subcooling can influence annual energy consumption. Cooling loads used for this analysis are the results of the study done by Armstrong et al. (2009b) for a typical office building in Chicago. The load scenarios are presented in terms of full-load-equivalent operating hours (FLEOH), as a function of part-load ratio and outside temperature. In Figure 17 *Load distribution A* represents instantaneous loads for a building without TES, while *load distribution B* represents loads that are shifted toward lower part-load ratios and lower outdoor temperatures using TES and daily optimized precooling. Load distribution B assumes hydronic radiant cooling, ideal thermal storage, a variable-speed chiller, and a dedicated outdoor air system for ventilation. Although the shifted load distribution will be affected by the exact performance characteristic of the heat pump or chiller, it is assumed that the distribution presented here is representative of the class of static-optimized machines with high-turndown variable-speed compressors, pumps, and fans.

The two cooling load scenarios may be convolved with several different heat pump configurations to estimate the influence of heat pump design on the annual energy consumption. Performance maps are created for the following heat pumps:

1. variable-speed compressor heat pump with optimized airflows and subcooling;
2. variable-speed compressor heat pump with optimized airflows, assuming zero subcooling;
3. variable-speed compressor heat pump with non-optimized airflows and subcooling (assuming zero subcooling and maximal airflows $V_z = 0.15\ \mathrm{m^3/s}$, $V_o = 0.77\ \mathrm{m^3/s}$);
4. two-speed compressor heat pump (assuming two-speed fans); and
5. dual variable-speed compressor heat pump with optimized airflows and subcooling.

For the heat pump with a two-speed compressor, subcooling is optimized for compressor speeds of $f = 0.5f_{\max}$ and $f = f_{\max}$. For this case, the fans were also assumed to be two-speed, with airflows set at the optimal values found for the variable-speed heat pump (Case 1) at $0.5Q_{\max}$ (used at the low-frequency compressor speed) and $Q_{\max}$ (used at the high-frequency speed). For part-load ratios other than $Q = 0.5Q_{\max}$ and $Q = Q_{\max}$, it has been

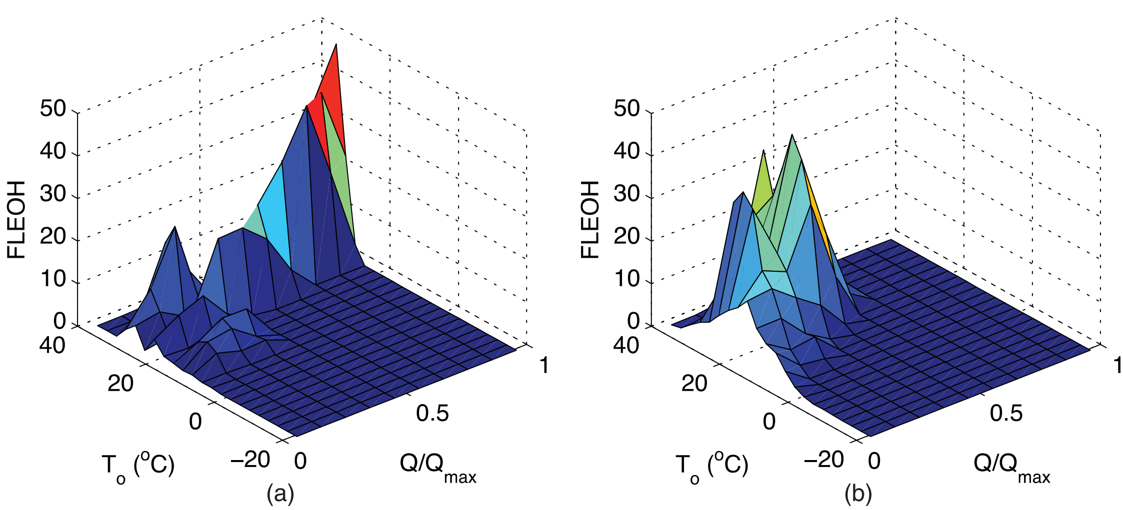

Figure 17. Sensible cooling load distribution for: (a) Case A (without TES) and (b) Case B (with TES) (color figure available online).

Table 1. Annual energy savings for different cases with R410A.

Optimized versus zero subcooling (B1 versus B2)	$(E_{zero\_sc} - E_{optimized})/E_{zero\_sc}$	0.4%
Optimized versus non-optimized (B1 versus B3)	$(E_{non\text{-}optimized} - E_{optimized})/E_{non\text{-}optimized}$	49.6%
Dual versus single compressor (B1 versus B5)	$(E_{single} - E_{dual})/E_{single}$	11.9%

assumed that the compressor cycles between $f = 0$, $f = 0.5f_{\max}$, and $f = f_{\max}$. The specific power (1/COP) for those cases is calculated using equations given in Armstrong et al. (2009a):

$$t_H = 2\frac{Q}{Q_{\max-1}}, \tag{5}$$

where t_H is the high-speed duty fraction: if $t_H < 0$,

if $t_H < 0$,

$$\frac{1}{\mathrm{COP}} = \frac{1}{\mathrm{COP\,(at\,T_o\,and\,}f = 0.5f_{\max})}; \tag{6}$$

else

$$\frac{1}{\mathrm{COP}} = (1 - t_H)\frac{1}{\mathrm{COP\,(at\,}T_o\mathrm{\,and\,}f = 0.5f_{\max})} + t_H\frac{1}{\mathrm{COP\,(at\,T_o\,and\,}f = f_{\max})}. \tag{7}$$

For cases 1 through 5, additional optimization was done for the refrigerant-side economizer mode. Combined heat pump maps, similar to the one in Figure 15 (compressor mode and economizer mode), were created using an algorithm that decides which mode uses less power for a given cooling load, zone, and outside temperature.

The annual energy consumption is calculated by convolving FLEOH distributions (distribution A or B) with different heat pump performance maps (Case 1–Case 5) as follows:

$$E = \sum_i \sum_j \mathrm{FLEOH}_{i,j}\frac{1}{\mathrm{COP}_{i,j}}Q_{\max}, \tag{8}$$

where *i,j* is the cell index in which *i* refers to the $Q/Q_{\max}$ grid and *j* refers to the T_o grid. Although FLEOH and the COP are generally functions of T_z, T_o, and part-load ratio ($Q/Q_{\max}$), in this analysis, fixed $T_z = 22°\mathrm{C}$ (71.6°F) is assumed.

Ten possible cases, A1-5 and B1-5, have been defined and introduce different refrigerants results in additional permutations. However, only several of the more interesting case results will now be described and compared.

The results presented in Table 1 show that with precooled TES, airflow optimization is considerably more important than subcooling optimization. The annual energy savings for the optimal case compared to the non-optimal case with fixed airflows and zero subcooling were around 50%. The savings were significantly less (around 0.4%) for the optimal case compared to the case with optimized airflows and zero subcooling. Table 1 also shows that a heat pump with two parallel compressors saves a significant amount of energy, especially for systems that operate at lower part-load ratios most of the time.

The results in Table 2 show that a variable-speed compressor heat pump (Case 1) achieves large energy savings compared to a two-speed compressor heat pump (Case 4), whether one is mostly operating at higher (distribution A) or at lower (distribution B) part-load ratios. Armstrong et al.'s study (2009a, 2009b) assumed a two-speed compressor heat pump for distribution A and a variable-speed compressor heat pump for distribution B. The results of this analysis (Table 2, column 4) show savings (around 20%) achieved by operating the heat pump at lower part-load ratios in addition to the variable-speed compressor savings (around 30%). However, as shown in Table 2, not all heat pumps benefit

Table 2. Annual energy savings for distribution A and distribution B using two-speed and variable-speed compressor heat pumps.

	A1 versus A4 $(E_{A4} - E_{A1})/E_{A4}$	B1 versus B4 $(E_{B4} - E_{B1})/E_{B4}$	A4 versus B1 $(E_{A4} - E_{B1})/E_{A4}$
R410	29.4%	34.5%	48.6%
Ammonia	20.1%	21.6%	38.3%
Propane	7.4%	12.6%	28.6%

Table 3. Annual energy savings for ammonia and propane with respect to R410A.

	A1 scenario $(E_{R410A} - E_{refrigerant})/E_{R410A}$	B1 scenario $(E_{R410A} - E_{refrigerant})/E_{R410A}$
Ammonia versus R410A	14.0	8.7%
Propane versus R410A	7.8	2.4%

equally from variable-speed compressor usage or operation at lower part-load ratios. For a better understanding of the heat pump power consumption when switching to different refrigerants (Table 3) the optimization algorithm presented here has shown to be extremely advantageous.

Using the same annual FLEOH distributions (Figure 17), an optimization is performed to find the heat pump sizing factor that minimizes energy consumption for scenarios A1 (distribution A with variable-speed heat pump), A4 (distribution A with two-speed heat pump), and B1 (distribution B with variable-speed heat pump). Figure 18 shows how different sizing factors influence the total annual energy savings compared to the nominal size system. The gradient-based optimization algorithm in MATLAB determined for this particular case that the optimal sizing factor for B1 would be 1.17, meaning that in this scenario, the heat pump has near-optimal size. Furthermore, the additional energy savings of the optimally sized system were very small compared to the nominally sized system. The heat pumps for A1 and A4 scenarios, on the other hand, are far from the optimum. The optimum that would be achieved with a 2.5 sizing factor for A1 and a 1.9 sizing factor for A4 would result in energy savings of approximately 20% for A1 and 17% for A4 compared to the nominal-sized system. Note that heat pump capital cost is not considered here, but also that the savings for an optimally sized heat pump are achieved almost entirely by increased evaporator and condenser size. Hence, its capital cost can be reduced without much impact on annual energy consumption by using a much smaller compressor (Arthur D. Little, Inc. [ADL] 2000; Levins et al. 1997).

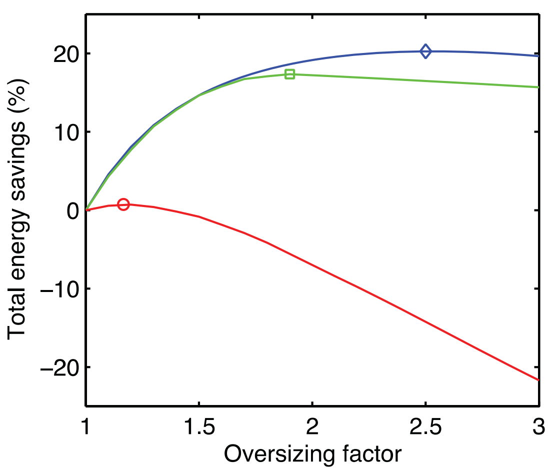

Figure 18. Heat pump optimal sizing for FLEOH distribution A with variable-speed heat pump (blue diamond), FLEOH distribution A with two-speed heat pump (green square), and FLEOH distribution B with variable-speed heat pump (red circle) (color figure available online).

Summary

An optimization algorithm that uses an adaptive grid search method is developed for heat pump static optimization over a wide range of conditions and loads. For a given cooling rate, zone, and outside temperature, the algorithm finds the optimal evaporator airflow, condenser airflow, and subcooling for which the total power consumption in minimal. All other heat pump parameters, such as the compressor frequency, refrigerant mass flow rate, temperatures, and pressures, are functions of the given inputs and optimization variables. The algorithm can be used to optimize an air-to-air, water-to-air, and water-to-water heat pump with any refrigerant supported by software REFPROP (Lemmon et al. 2007). It can also be used for different heat pump types, such as heat pumps with a single or multiple evaporators, compressors, and condensers, heat pumps with single-, two-, or variable-speed compressors, as well as heat pumps with different compressor types. Although only sensible cooling optimization results were presented here, the heat pump model developed by Zakula et al. (2011) can also be used to optimize simultaneous sensible and latent cooling.

The optimization results for an air-to-air heat pump with a single rolling-piston compressor and R410A as a working fluid have been presented over a wide range of conditions and loads. It is shown that the COP and optimal subcooling are almost solely functions of a part-load ratio and temperature difference between a zone and outside. It has also been shown that the COP increases for lower part-load ratios, which suggests that modest oversizing of optimally controlled variable-speed heat pumps is desirable.

The case with zero subcooling and optimized airflows has been compared to the fully optimized heat pump performance. Although relatively small (0–5%), the COP benefits of subcooling increase for higher part-load ratios and larger temperature differences. The importance of airflow optimization was demonstrated, analyzing the case with fixed airflows, in which case the COP values were significantly lower compared to the optimal case. Furthermore, the results show that a heat pump primarily optimized for simultaneous sensible cooling and dehumidification can significantly underperform when used for sensible cooling only in, for example, an application where dedicated outdoor air system (DOAS) handles latent loads.

The specific power of a heat pump with a single compressor increases for very low part-load ratios (less than 0.2 in this example), mainly because of inverter losses. One of the possible improvements analyzed here is a heat pump with two parallel compressors. For part-load ratios lower than 0.5, the control algorithm decides if it is more efficient to run one or two compressors, while for the higher part-load ratios, both compressors operate in parallel. The results of this analysis show significant improvement at lower part-load ratios when two parallel compressors are used.

Although an economizer mode can be used when the outside temperature is lower than the inside temperature, it has been shown that the economizer mode is not always more economical. The optimization algorithm can be used here to decide whether the compressor mode or economizer mode uses the least amount of energy.

Using the optimization algorithm, it is possible to predict the performance of a heat pump when switching to different refrigerants. This was demonstrated by comparing the power consumption of ammonia and propane heat pumps against an R410A heat pump.

The annual energy consumption has been compared among different cases using the sensible cooling load distribution for a typical office in Chicago. For this particular example, the system with optimized variables annually saves approximately 50% of energy compared to the non-optimized system, which indicates the importance of heat pump static optimization and the model predictive control of TES. The system with a variable-speed compressor that operates at night by precooling and at lower part-load ratios most of the time saves a significant amount of energy compared to the system with two-speed compressor that operates at higher part-load ratios. It is also shown that the system can benefit from a heat pump with two compressors that work in parallel, since this reduces inverter losses at low part-load ratios. Furthermore, optimization has been used to find the optimal heat pump sizing. The shape of oversizing curves and the optimal size are shown to be very dependent on a particular application. For the system that operates at higher part-load ratios most of the time, the optimal sizing resulted in approximately 17–20% annual energy saving compared to the nominal system size.

In conclusion, the algorithm presented here can be used to optimize heat pump performance over a wide range of operating conditions and loads. The gradient method was then used to find an optimal heat pump sizing for a particular application. These procedures are particularly beneficial for novel systems, for which curve fits to the optimization results could easily be implemented as a part of a building predictive control. The algorithm can also be used to analyze the influence of different optimization variables or to compare heat pumps with a different combination of components or different refrigerants.

Acknowledgments

The authors wish to acknowledge the MIT Energy Initiative, the Masdar Institute of Science and Technology, the National Science Foundation (EFRI-SEED award 1038230), and the Martin Family Society of Fellows for Sustainability for their support of this research. They also thank Pacific Northwest National Laboratory for sharing the results of its study of low-lift cooling technology, Eric Lemmon from the National Institute of Standards and Technology for his support with the software REFPROP, and Dr. Piotr Domanski for his help regarding the appropriate sizing when switching to different refrigerants.

Nomenclature

COP = coefficient of performance (—)
D = compressor displacement, m^3 (ft^3)
E = energy, J (Btu)

f = compressor shaft speed, Hz
h = enthalpy, J/kg (Btu/lb)
J = power, W (Btu/hr)
Q = cooling rate, W (Btu/hr)
T = temperature, °C (°F)
t_H = high-speed duty fraction (—)
y = condenser area percentage (—)
ρ = refrigerant density at suction conditions, kg/m^3 (lb/ft^3)

Subscripts

c,avg = average condensing
e,avg = average evaporating
lg = refers to change from saturated liquid to saturated vapor
max = maximal
o = outside
opt = optimal
sc = subcooling region of condenser
z = zone

References

Arthur D. Little, Inc. (ADL). 2000. *Energy efficient rooftop air conditioner: Continuation application technical progress statement*. Project DE-FC26-99FT40640, Cambridge, MA: Arthur D. Little, Inc..

Armstrong, P.R., W. Jiang, D.W. Winiarski, S. Katipamula, L.K. Norford, and R.A. Willingham. 2009a. Efficient low-lift cooling with radiant distribution, thermal storage and variable-speed chiller controls—Part I: Component and subsystem models. *HVAC&R Research* 15(2):366–401.

Armstrong, P.R., W. Jiang, D.W. Winiarski, S. Katipamula, L.K. Norford, and R.A. Willingham. 2009b. Efficient low-lift cooling with radiant distribution, thermal storage and variable-speed chiller controls—Part II: Annual energy use and savings. *HVAC&R Research* 15(2):402–32.

ASHRAE. 2009. *2009 ASHRAE Handbook—Fundamentals*. ASHRAE, Atlanta, GA.

ASHRAE. 2011. *2011 ASHRAE Handbook—Applications*. ASHRAE, Atlanta, GA.

Braun, J.E. 2007. Near-optimal control strategies for hybrid cooling plans. *International Journal of HVAC&R Research* 13(4):599–622.

Braun. J.E., S.A. Klein, W.A. Beckman, and J.W. Mitchell. 1989. Methodologies for optimal control of chilled water systems without storage. *ASHRAE Transactions* 95(1):652–62.

Braun, J.E., J.W. Mitchell, and S.A. Klein. 1987a. Performance and control characteristics of a large cooling systems. *ASHRAE Transactions* 93(1):1830–52.

Braun, J.E., J.W. Mitchell, and S.A. Klein. 1987b. Models for variable-speed centrifugal chillers. *ASHRAE Transactions* 93(1):1974–813.

Domanski, P.A. 1995. Minimizing throttling losses in the refrigeration cycle. *Proceedings of the International Congress of Refrigeration, International Institute of Refrigeration, Paris, France*, pp. 766–73.

Gayeski, N. 2010. *Predictive pre-cooling control for low lift radiant cooling using building thermal mass*. Doctoral dissertation, Massachusetts Institute of Technology, Cambridge, MA.

Gayeski, N.T., T. Zakula, P.R. Armstrong, and L.K. Norford. 2011. Empirical modeling of a rolling-piston compressor heat pump for predictive control in low-lift cooling. *ASHRAE Transactions* 117(2).

Jiang, W., and T.A. Reddy. 2007. Combining engineering optimization of primary HVAC&R plants with decision analysis methods—Part I: Deterministic analysis. *HVAC&R Research* 13(1):93–117.

Jiang, W., D. Winiarski, S. Katipamula, and P.R. Armstrong. 2007. *Cost-effective integration of efficient low-lift base load cooling equipment*. PNNL-17157, Pacific Northwest National Laboratory, Richland, WA.

Katipamula S., P.R. Armstrong, W. Wang, N. Fernandez, H. Cho, W. Goetzler, J. Burgos, R. Radhakrishnan, and C. Ahlfeldt. 2010. *Cost-effective integration of efficient low-lift baseload cooling equipment–FY08 Final Report PNNL-19114*. Pacific Northwest National Laboratory, Richland, WA.

King, D.J., and R.A. Potter. 1988. Description of a steady-state cooling plant model developed for use in evaluating optimal control of ice thermal energy storage systems. *ASHRAE Transactions* 104(1):42–53.

Klein, S.A., W.A. Beckman, L. Broman, A. Fiksel, E. Linberg, M. Schuller, and J. Thorton. 2010. *TRNSYS 17: A transient system simulation program. Solar Energy Laboratory*, University of Wisconsin. Madison, WI. http://sel.me.wisc.edu/trnsys.

Lau, A.S., W.A. Beckman, and J.W. Mitchell. 1985. Development of computer control—Routines for a large chilled water plant. *ASHRAE Transactions* 91(1):780–91.

Lemmon, E.W., M.L. Huber, and M.O. McLinden. 2007. *NIST Standard Reference Database 23: Reference Fluid Thermodynamic and Transport Properties-REFPROP*, Version 8.0. National Institute of Standards and Technology, Standard Reference Data Program, Gaithersburg, MD.

Levins, W.P., C.K. Rice, and V.D. Baxter. 1997. Modeled and measured effects of compressor downsizing in an existing air conditioner/heat pump in the cooling mode. *ASHRAE Transactions* 192(2):22–33.

New Technology Demonstration Program (NTDP). 1994. *Federal technology alert: liquid refrigerant pumping*. Report PNL-10232, Pacific Northwest National Laboratory, Richland, WA.

Verhelst, C., F. Logist, J.V. Impe, and L. Helsen. 2012. Study of the optimal control problem formulation for modulating air-to-water heat pumps connected to a residential floor heating system. *Energy and Buildings* 45:43–53.

Zakula, T. 2010. *Heat pump simulation model and optimal variable-speed control for a wide range of cooling conditions*. Master thesis. Massachusetts Institute of Technology.

Zakula, T., N.T. Gayeski, P.R. Armstrong, and L.K. Norford. 2011. Variable-speed heat pump model for a wide range of cooling conditions and loads. *HVAC&R Research* 17(5):670–91.